

Light-scattering form factors of asymmetric particle dimers from heteroaggregation experiments

Paolo Galletto and Wei Lin

Department of Inorganic, Analytical, and Applied Chemistry, University of Geneva, 1211 Geneva 4, Switzerland

Michael I. Mishchenko

National Aeronautics and Space Administration (NASA) Goddard Institute for Space Studies, 2880 Broadway, New York, New York 10025

Michal Borkovec^{a)}

Department of Inorganic, Analytical, and Applied Chemistry, University of Geneva, 1211 Geneva 4, Switzerland

(Received 22 February 2005; accepted 15 June 2005; published online 16 August 2005)

Measurements of form factors of asymmetric particle dimers composed of oppositely charged polystyrene latex particles are presented. These measurements are based on time-resolved static and dynamic light scattering on dilute aggregating aqueous suspensions. The experimental form factors are compared with independent calculations based on the superposition T -matrix method and Rayleigh-Debye-Gans (RDG) approximation. While the RDG approximation is found to be reliable only up to particle diameters of about 250 nm, the superposition T -matrix method is very accurate for all types of dimers investigated. The present results show clearly the appropriateness of the superposition T -matrix method to estimate the optical properties of colloidal particles in the micrometer range reliably. © 2005 American Institute of Physics. [DOI: 10.1063/1.1996570]

INTRODUCTION

Scattering of light from particle aggregates in the micrometer size range is essential in a variety of systems, including suspensions, emulsions, clouds, or dust. In order to understand the optical properties of these systems, one must be able to predict the optical response of particle aggregates. Such predictions are indispensable for a wide variety of scientific fields. Let us just mention two very different examples. First, in the development of novel materials, functionalized latex particles, coated metal particles, or polymeric capsules are relevant.^{1–4} Thereby, light scattering is commonly used to monitor the aggregation state of such suspensions.^{5–9} In order to measure the particle-aggregation rate constants reliably, it is important to be able to predict the optical response of particle aggregates. Second, consider the analysis of global satellite observations.^{10,11} The model and the satellite retrieval results depend critically on the albedo caused by the particulate matter in the atmosphere. Again, the reliable prediction of the optical properties of particle aggregates becomes a central issue.

In the past, the calculation of optical properties of an object was approached based on the classical theory of Rayleigh-Debye-Gans (RDG).^{12,13} This theory is applicable when the particle or aggregate size is small compared to the wavelength of light, or when the contrast is sufficiently weak. In many situations, however, these conditions are not met, and an exact solution of Maxwell's equations becomes necessary. Such an exact solution has been put forward by

Mie around the turn of the century for a sphere, but analogous solutions for other geometries have remained inaccessible until relatively recently. Among those, the coupled dipole approximation can handle objects of any shape. Thereby, the object is replaced by an array of dipoles, and as a result, the technique is computationally expensive, particularly, when averaging over orientations become necessary.^{14,15} Techniques based on T -matrix methods are much more powerful for aggregates composed of spherical particles. Here one obtains the exact solution based on expansions in spherical harmonics, and the currently implemented codes are fast, accurate, and provide orientation-averaged results directly.^{16,17}

Nevertheless, in order to be able to apply these techniques to realistic systems, it is necessary to gain confidence in these approaches by comparing their predictions with experimental results on well-defined model systems. Initially, such tests were carried out in the microwave region, where the scattering could be directly tested on macroscopic objects.^{18,19} More recently, such a comparison was carried out in the optical regime on individual aggregates composed of a few primary particles, but some uncertainties concerning the particle size, which was supplied by the manufacturer, remained.²⁰

A different approach to study the properties of particle dimers in the optical regime is to focus on the initial stages of an aggregating suspension of colloidal particles. This type of comparison was so far carried out for identical particles,⁶ but mixed systems composed of different particles provide a more stringent test, as asymmetric particle dimers could be studied. Such an analysis is being put forward here. The

^{a)}Author to whom correspondence should be addressed; electronic mail: michal.borkovec@unige.ch

heteroaggregation of two oppositely charged particles is followed by time-resolved simultaneous static and dynamic light scattering (SSDLS), and from its initial time dependence we extract the form factor of the dimers. While the systems investigated show substantial deviations to the RDG theory, the superposition T -matrix method captures the experimental data very well.

THEORY

Let us first discuss the scattering from a dilute binary colloidal suspension where asymmetric particle dimers form by heteroaggregation, and then discuss how the optical properties of these dimers can be calculated.

Light scattering from early stages of heteroaggregation

Consider colloidal suspension composed of spherical particles A and B , which exclusively undergoes heteroaggregation. In the early stages of the aggregation process, only particle dimers AB are forming according to the kinetic process $A+B \rightarrow AB$. This situation has been discussed earlier in more detail,²¹ and only a summary is given here for completeness. The concentrations of the components follow the kinetic equations

$$\frac{dN_{AB}(t)}{dt} = -\frac{dN_A(t)}{dt} = -\frac{dN_B(t)}{dt} = k_{AB}N_A(t)N_B(t), \quad (1)$$

where $N_i(t)$ is the time-dependent particle number concentrations of species i ($i=A, B, AB$) and k_{AB} is the heteroaggregation rate constant.

In a static light-scattering experiment, the intensity of the scattered light varies with time due to the formation of aggregates. In the case of a dilute aggregating suspension, it is given by

$$I(q, t) = \sum_i I_i(q)N_i(t), \quad (2)$$

where $I_i(q)$ is the static light-scattering intensity of the species $i=A, B, AB$, and q is the magnitude of the scattering vector given by $q=(4\pi/\lambda)\sin(\theta/2)$, where λ is the wavelength of the light in the medium and θ is the scattering angle. The relative change in static light-scattering intensity can be obtained by differentiating Eq. (2) and inserting into Eq. (1). One obtains the result

$$\frac{1}{I(q, 0)} \frac{dI(q, t)}{dt} \Big|_{t \rightarrow 0} = \frac{k_{AB}N_0x_Ax_B[I_{AB}(q) - I_A(q) - I_B(q)]}{I_A(q)x_A + I_B(q)x_B}, \quad (3)$$

where $I(q, 0) = I_A(q)N_A(0) + I_B(q)N_B(0)$ is the initial scattering intensity, $N_0 = N_A(0) + N_B(0)$ is the initial total particle number concentration, and $x_i = N_i(0)/N_0$ is the initial number fraction of particle i ($i=A, B$).

Dynamic light scattering measures the average diffusion coefficient of the species present, weighted by the scattered light intensity. In a dilute binary colloidal system, the apparent diffusion coefficient is

$$D(t) = \frac{\sum_i D_i I_i(q) N_i(t)}{\sum_i I_i(q) N_i(t)}, \quad (4)$$

where D_i is the diffusion coefficient of species i ($i=A, B, AB$). By taking the time derivative of Eq. (4) and combining with Eqs. (1) and (2), we obtain the relative rate of change of the diffusion coefficient

$$\begin{aligned} \frac{1}{D(0)} \frac{dD(q, t)}{dt} \Big|_{t \rightarrow 0} &= k_{AB}N_0x_Ax_B \left[\frac{D_{AB}I_{AB}(q) - D_A I_A(q) - D_B I_B(q)}{D_A I_A(q)x_A + D_B I_B(q)x_B} \right. \\ &\quad \left. - \frac{I_{AB}(q) - I_A(q) - I_B(q)}{I_A(q)x_A + I_B(q)x_B} \right], \end{aligned} \quad (5)$$

where

$$D(0) = \frac{D_A I_A(q)x_A + D_B I_B(q)x_B}{I_A(q)x_A + I_B(q)x_B} \quad (6)$$

is the initial value of the apparent diffusion coefficient. The isotropically averaged diffusion coefficient of the dimer can be expressed as

$$D_{AB} = \frac{2}{\alpha} \frac{D_A D_B}{D_A + D_B}, \quad (7)$$

where the relative hydrodynamic radius of the dimer α is given by the approximation formula²¹

$$\alpha = 1.392 + 0.608 \left(\frac{r_B - r_A}{r_B + r_A} \right)^2, \quad (8)$$

where r_i is the radius of particle i ($i=A, B$). This formula agrees to a few percent with the exact solution obtained from the flow around two spheres at low Reynolds numbers.

Computation of form factors of asymmetric dimers

The angular dependence of the scattered intensity of a scatterer i is commonly expressed in terms of the form factor

$$P(q) = \frac{I_i(q)}{I_i(0)}. \quad (9)$$

The form factor is a dimensionless quantity with the property $P(0)=1$. The scattering intensity of an asymmetric dimer of two spherical particles A and B can be expressed within the RDG approximation as

$$I_{AB}(q) = I_A(q) + I_B(q) + 2\sqrt{I_A(q)I_B(q)} \frac{\sin q(r_A + r_B)}{q(r_A + r_B)}, \quad (10)$$

where the scattering intensity of the monomer is given by

$$I_i(q) \propto \frac{1}{q^6} [\sin qr_i - q r_i \cos qr_i]^2. \quad (11)$$

These expressions are only applicable for particles which are sufficiently small compared to the wavelength of the light, or at sufficiently weak contrast.

For larger particles, the scattered intensity of asymmetric doublets must be computed using an exact solution of the Maxwell equations. We have used the so-called superposition T -matrix method as described earlier.¹⁷ The gist of this technique can be summarized as follows. Consider scattering of a plane electromagnetic wave by an arbitrary fixed multi-sphere aggregate. The incident and the total scattered electric fields at an observation point are expanded in vector spherical wave functions (VSWFs) centered at the origin of the coordinate system

$$\mathbf{E}^{\text{inc}}(\mathbf{r}) = \sum_{n=1}^{\infty} \sum_{m=-n}^n [a_{mn} \text{Rg}\mathbf{M}_{mn}(k\mathbf{r}) + b_{mn} \text{Rg}\mathbf{N}_{mn}(k\mathbf{r})], \quad (12)$$

$$\mathbf{E}^{\text{sca}}(\mathbf{r}) = \sum_{n=1}^{\infty} \sum_{m=-n}^n [p_{mn} \mathbf{M}_{mn}(k\mathbf{r}) + q_{mn} \mathbf{N}_{mn}(k\mathbf{r})], \quad (13)$$

where $k=2\pi/\lambda$ is the wave number in the surrounding medium and \mathbf{r} is the position vector of the observation point. The coordinate system can be chosen arbitrarily, although it is advantageous to place its origin at the geometrical center of the cluster. The properties of the vector spherical wave functions are summarized in Appendix C of Ref. 13. The functions $\text{Rg}\mathbf{M}_{mn}$ and $\text{Rg}\mathbf{N}_{mn}$ are regular (finite) at the origin, while the use of the outgoing functions \mathbf{M}_{mn} and \mathbf{N}_{mn} in Eq. (13) ensures that the scattered field satisfies the radiation condition at infinity (i.e., the transverse component of the scattered electric field decays as $1/r$, whereas the radial component decays faster than $1/r$ with $r \rightarrow \infty$).

The expansion coefficients of the plane incident wave are given by simple closed-form analytical expressions and can be easily evaluated. Owing to the linearity of the Maxwell equations and constitutive relations, the relation between the scattered-field expansion coefficients p_{mn} and q_{mn} on one hand and the incident field expansion coefficients a_{mn} and b_{mn} on the other hand must be linear and is given by the so-called transition matrix (or T matrix) \mathbf{T} as follows:

$$p_{mn} = \sum_{n'=1}^{\infty} \sum_{m'=-n'}^{n'} (T_{mm'n'n'}^{11} a_{m'n'} + T_{mm'n'n'}^{12} b_{m'n'}), \quad (14)$$

$$q_{mn} = \sum_{n'=1}^{\infty} \sum_{m'=-n'}^{n'} (T_{mm'n'n'}^{21} a_{m'n'} + T_{mm'n'n'}^{22} b_{m'n'}). \quad (15)$$

In compact matrix notation, Eqs. (14) and (15) can be rewritten as

$$\begin{bmatrix} \mathbf{p} \\ \mathbf{q} \end{bmatrix} = \mathbf{T} \begin{bmatrix} \mathbf{a} \\ \mathbf{b} \end{bmatrix} = \begin{bmatrix} \mathbf{T}^{11} & \mathbf{T}^{12} \\ \mathbf{T}^{21} & \mathbf{T}^{22} \end{bmatrix} \begin{bmatrix} \mathbf{a} \\ \mathbf{b} \end{bmatrix}, \quad (16)$$

which means that the column vector of the expansion coefficients of the scattered field is obtained by multiplying the T matrix and the column vector of the expansion coefficients of the incident field.

To compute the T matrix, the total field scattered by the cluster, $\mathbf{E}^{\text{sca}}(\mathbf{r})$, is expressed as a superposition of individual fields scattered from each sphere. The individual fields

scattered by the component spheres are expanded in VSWFs, with origins at the individual sphere centers. The linear relation between the corresponding expansion coefficients and the incident-wave expansion coefficients a_{mn} and b_{mn} is established via the diagonal individual-sphere T matrices, with elements given by the corresponding Lorenz-Mie coefficients. This procedure ultimately results in a matrix equation for the scattered-field expansion coefficients of each sphere. Inversion of this cluster matrix equation gives sphere-centered transition matrices that transform the expansion coefficients of the incident wave into the expansion coefficients of the individual scattered fields. In the far-field zone of the entire cluster, the individual scattered-field expansions are transformed into a single expansion centered at the common origin of the cluster. This procedure gives the cumulative T matrix of the cluster, which enters Eq. (16).

Equation (16) is the cornerstone of the T -matrix approach. Indeed, if the T matrix is known, Eqs. (12)–(15) give the scattered field and any observable scattering characteristic of the cluster can be evaluated. Furthermore, the T matrix can be used in an analytical averaging of scattering characteristics over cluster orientations,^{13,16,17} which makes this technique orders of magnitude faster than any alternative exact solution of Maxwell's equations.

The T -matrix computer code used in our computations is described in Sec. 5.13 of Ref. 13 and is available at www.giss.nasa.gov/~crmim. The code yields all scattering and absorption characteristics of a two-sphere cluster in random orientation, including the extinction, scattering, and absorption cross sections, the single-scattering albedo, the asymmetry parameter, and the elements of the normalized Stokes scattering matrix. In particular, the product of the scattering cross section and the (1,1) element of the scattering matrix determines the scattered intensity $I_{AB}(q)$. The code has been thoroughly tested and gives very accurate results within the domain of numerical convergence. Unlike the case with the RGD approximation, which is fully analytic, the practical use of the T -matrix technique may require significant computer resources. However, the decisive advantage of the T -matrix method is that it is numerically exact and generates guaranteed numbers for any refractive index and particle size as long as numerical convergence is reached.

EXPERIMENT

Light-scattering instrumentation

The instrument used is a multiangle simultaneous static and dynamic light-scattering (SSDLS) goniometer equipped with eight optical fiber detectors (ALV/CGS-8, Langen, Germany) with a solid-state laser operating at 532 nm (Verdi V2, Coherent) as a light source. The optical fibers guide light to photomultipliers and the output signals are fed into correlator boards, which accumulate the autocorrelation functions and the scattered intensities from all detectors. By rotating the goniometer during the measurement, additional scattering angles can be monitored, thus increasing the angular resolution.

TABLE I. Summary of the particle properties. Measured diameters and polydispersity expressed as coefficient of variation (CV) by transmission electron microscopy (TEM). Hydrodynamic and gyration diameters are measured by dynamic and static light scattering (DLS and SLS), respectively. The best-fitted diameters used in the calculations and charging properties of the particles are given as well.

Code	Type	Diameter (nm)				CV		Charging characteristics	
		Best	TEM ^a	SLS	DLS	TEM ^a	SLS	Charge ^a (mC/m ²)	Mobility ^b (10 ⁻⁸ m ² V ⁻¹ s ⁻¹)
S282	Sulfate	282	270	274	290	0.06	0.09	11	-3.9
S358	Sulfate	358	350	355	360	0.03	0.07	12	-4.5
A160	Amidine	160	133	160	160	0.11	...	82	+4.3
A220	Amidine	220	214	220	220	0.08	...	100	+4.4
A482	Amidine	482	472	473	490	0.03	0.05	160	+4.7

^aDetermined by the manufacturer.

^bMeasured in 10⁻⁴M HCl.

Particle characterization and sample preparation

Sulfate- and amidine-terminated surfactant *T*-free polystyrene latex particles were purchased from Interfacial Dynamics Corporation (IDC, Portland). Before use, the latex particles were dialyzed for about two weeks in de-ionized water (Milli-Q, Millipore) until the conductivity of the surrounding water decreased to that of the pure de-ionized water. The particle concentration was determined by total carbon analysis (TOCV, Shimadzu) or by comparison of the scattered intensities with a reference sample as obtained by static light scattering. Electrophoretic mobilities were measured by laser doppler velocimetry (Zetasizer 2000, Malvern). From these measurements, we have verified the expected sign of the particle charge (see Table I).

Glass cuvettes used for light scattering were cleaned in hot mixture of H₂O₂ and H₂SO₂ (1:4), rinsed excessively with de-ionized water, and rinsed with a suspension of amidine latex to reduce loss of sample on cuvette walls. The samples were prepared by diluting the dialyzed suspensions with de-ionized water. The solution was adjusted to pH 4 with HCl, resulting in an ionic strength of 10⁻⁴M.

Particle size was determined by analyzing dilute suspensions of each individual type of particles by static and dynamic light scattering. The total particle concentration was adjusted to 2 × 10¹⁴ m⁻³, which corresponds to a mass concentration ranging from 0.4 to 4 mg/L. Form factors shown in Fig. 1 were found by dividing the measured scattering intensity $I(q)$ by the forward-scattering intensity $I(q=0)$ obtained by extrapolation to small q in a Guinier plot. The static light-scattering data could be fitted well to a model of a polydisperse suspension with Mie theory, including a correction for the reflected light (see Fig. 1). The size distribution was assumed a truncated Gaussian, and the Mie scattering functions were evaluated according to standard procedures.^{12,13} The calculations used a refractive index for the latex particles of 1.596 (polystyrene) and 1.337 for the solvent (water), and a reflection coefficient of 0.059, the latter being defined as the ratio between the magnitudes of the incident and reflected electric fields.⁶ These parameters could be used for all latex samples, and were further employed in the superposition *T*-matrix calculations. Dynamic light scattering was analyzed with second-order cumulant fit, and one

obtains a constant hydrodynamic radius within the error of a few percent with the exception near the minima of the form factor. These findings, summarized in Table I, are in good agreement with the manufacturer's specifications.

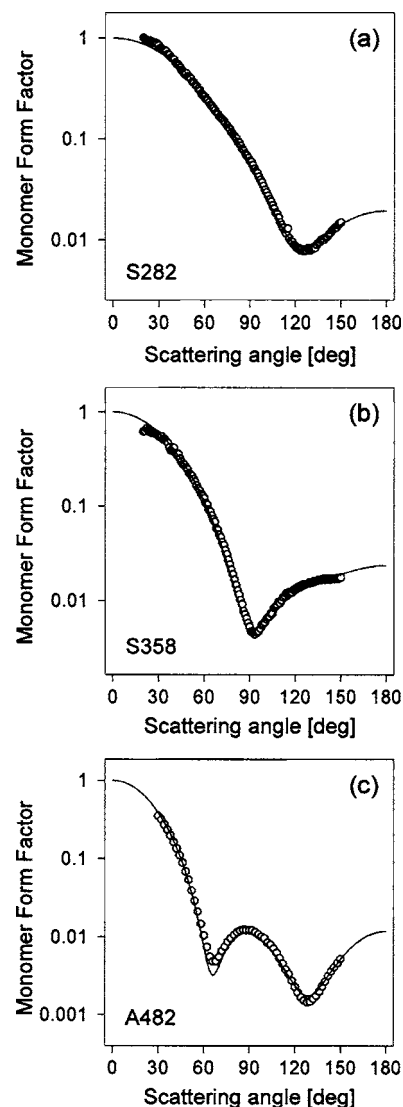


FIG. 1. Monomer form factors of the larger particles used with best fit by Mie theory including polydispersity and back-reflection correction. (a) S282, (b) S358, and (c) A482.

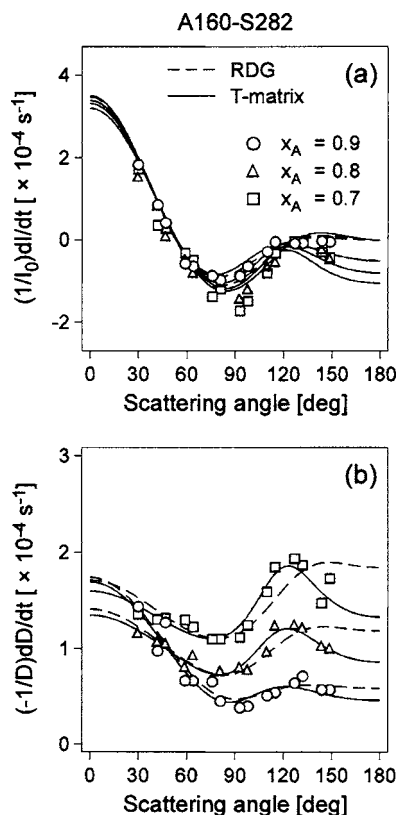


FIG. 2. Experimentally observed apparent rates for the couple A160-S282 together with the best fit using the T -matrix calculations (solid) and RDG approximation (dashed). The mole fraction of amidine particles is denoted by x_A . (a) Static and (b) dynamic light scattering.

Time-resolved aggregation studies

Samples for heteroaggregation studies were prepared by mixing dilute suspensions of respective amidine and sulfate latex particles in $10^{-4}M$ HCl solution in order to maintain the ionic strength and pH of 4. Formation of particle aggregates was monitored by time-resolved SSDLS with an angular resolution of 8° for about 20 min. For the largest particle couple studied (A482-S358), the angular resolution could be decreased to 5° , since the aggregation kinetics was sufficiently slow. The correlation functions were typically accumulated for 20 s, and were analyzed with a second-order cumulant fit. Formation of aggregates could be evidenced by the increase of the scattering intensity at sufficiently low angles, and a decrease of the apparent diffusion coefficient. The initial rate of change of both quantities was extracted as a function of the scattering angle. For the chosen particle concentration, the initial diffusion coefficient was in good agreement with Eq. (6) and showed a relative decrease of about 20%. From this observation, we conclude that the system is indeed in the early stages of the aggregation, and that formation of larger aggregates can be neglected. The same conclusion can be obtained by estimating the half-time of the aggregation $T_{1/2} \approx 2/(k_{AB}N_0)$ and approximating the rate constant by Smoluchowski's value of $12 \times 10^{-18} \text{ m}^3/\text{s}$. The half-time is around 800 s, which is comparable to the experimental time window. From similar studies on suspensions of the individual latex particles, we have verified that no homoaggregation could be observed under the same conditions.

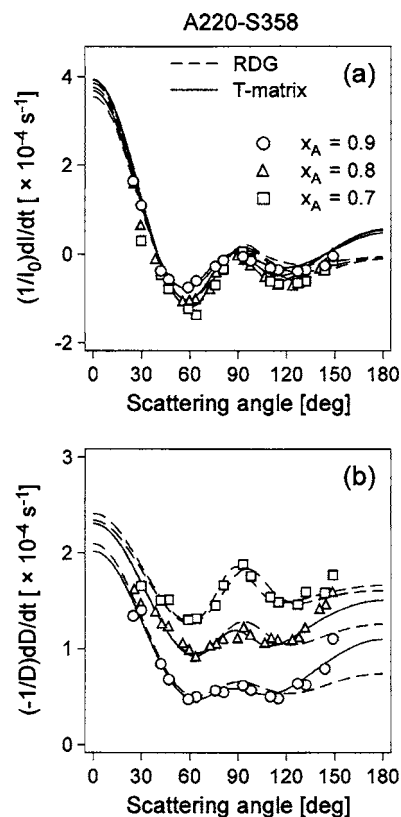


FIG. 3. Experimentally observed apparent rates for the couple A220-S358 together with the best fit using the T -matrix calculations (solid) and RDG approximation (dashed). The mole fraction of amidine particles is denoted by x_A . (a) Static and (b) dynamic light scattering.

RESULTS AND DISCUSSION

Three different binary mixtures of oppositely charged particles undergoing exclusive heteroaggregation were used, namely, A160-S282, A220-S358, and A482-S358. The particle properties are summarized in Table I. Absolute heteroaggregation rate constants have been determined in an electrolyte solution at an ionic strength of $10^{-4}M$. The apparent SLS and DLS rate constants are shown in Figs. 2–4.

Absolute aggregation rate constants

The rate constants were determined in two different ways. The first approach incorporates the evaluation of the apparent rate constants given by Eqs. (3) and (5) with the scattering functions of the particle dimer with the superposition T -matrix method in a least-squares-fitting algorithm. From the SLS data, we have extracted the absolute aggregation rate constant k_{AB} , while to the DLS data the relative hydrodynamic dimer radius α was fitted as well. The results for the three pairs A160-S282, A220-S358, and A482-S358 are summarized in Table II. The corresponding fits of the experimental data are shown in Figs. 2–4 (solid lines). The RDG approximation (dashed lines) gives a worse description of the data. In particular, the DLS data for the pairs A160-S282 and A482-S358 are poorly described [Figs. 2(b) and 3(b)].

The second approach does not rely on any optical models. Here we shall only summarize the essence of the tech-

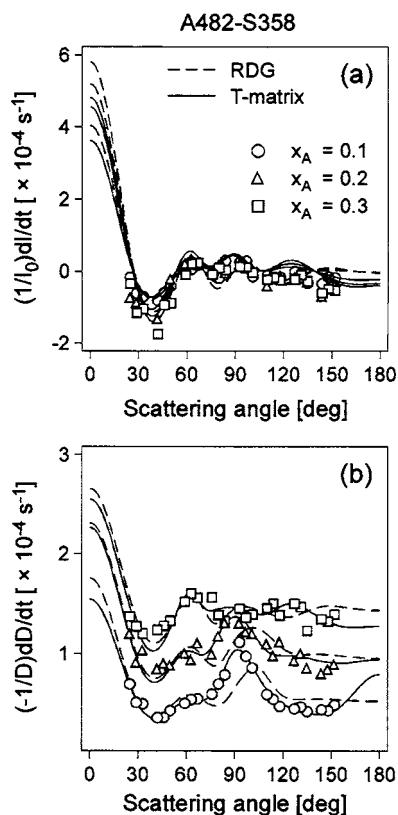


FIG. 4. Experimentally observed apparent rates for the couple A482-S358 together with the best fit using the T -matrix calculations (solid) and RDG approximation (dashed). The mole fraction of amidine particles is denoted by x_A . (a) Static and (b) dynamic light scattering.

nique, as the details can be found in a separate publication.²² The technique is based on the measurement of SSDLS. From these data, the aggregation rate as well as the hydrodynamic dimer radius can be extracted without making any assumptions concerning the form factor of the dimer. While the technique has the advantage to be model free, it has the disadvantage to be accompanied with larger errors than the previous one. Moreover, we had problems with the convergence of the technique, albeit not for the examples

shown here. The corresponding results are summarized in Table II. One immediately observes that these SSDLS results are well consistent with the independent analysis of the SLS and DLS results, which rely on the superposition T -matrix method.

Both approaches give very similar results for the rate constants, and they further are independent of the mole fraction used. For the couples A160-S282, A220-S358, and A482-S358, our best estimates of the heteroaggregation rate constants are $(6.8 \pm 0.4) \times 10^{-18} \text{ m}^3 \text{ s}^{-1}$, $(6.4 \pm 0.4) \times 10^{-18} \text{ m}^3 \text{ s}^{-1}$, and $(6.4 \pm 0.7) \times 10^{-18} \text{ m}^3 \text{ s}^{-1}$, respectively. These values are comparable to earlier measurements of absolute rate constants for heteroaggregation of smaller particles under similar conditions,²¹ and they are somewhat smaller than the diffusion-controlled rate constant of $12 \times 10^{-18} \text{ m}^3 \text{ s}^{-1}$ given by the classical Smoluchovski theory. This difference is mainly caused by the presence of the hydrodynamic interactions between the approaching spheres, which causes a slowdown of the aggregation process.

Very similar values for the relative hydrodynamic dimer radius are also obtained from the two techniques, and for this reason the best-fitted values can be obtained from their averages, namely, 1.40 ± 0.07 , 1.46 ± 0.07 , and 1.33 ± 0.05 for the couples A160-S282, A220-S358, and A482-S358, respectively. These values should be compared with the corresponding theoretical estimates of 1.44, 1.43, and 1.40 [cf. Eq. (8)]. All these estimates are within the error margins, with the exception of the largest couple A482-S358, where the hydrodynamic radius is overestimated by theory. This disagreement is similar to the results reported for homoaggregation.⁶ This minor discrepancy is eventually due to contributions from rotational diffusion in the DLS signal, which is expected to become more important for large particles.

We note that the results of the model-free analysis agree very well with those obtained by the T -matrix method. While the model-free analysis makes no assumptions about the optical properties of the dimer, the agreement of both tech-

TABLE II. Measured heteroaggregation rate constants and relative hydrodynamic radii for the couples investigated. The mole fraction of amidine particles is denoted by x_A .

Couple	x_A	$k_{AB} (\times 10^{-18} \text{ m}^3 \text{ s}^{-1})$			α		
		SLS	DLS	SSDLS	DLS	SSDLS	Theory
A160-S282	0.7	6.84 ± 0.45	6.76 ± 0.30	7.08 ± 0.51	1.43 ± 0.07	1.42 ± 0.07	
	0.8	6.48 ± 0.42	6.86 ± 0.30	6.96 ± 0.60	1.37 ± 0.07	1.38 ± 0.07	
	0.9	6.92 ± 0.34	6.63 ± 0.42	6.54 ± 0.96	1.40 ± 0.07	1.41 ± 0.08	
Average		6.7 ± 0.4	6.8 ± 0.4	6.9 ± 0.7	1.40 ± 0.07	1.40 ± 0.07	1.44
A220-S358	0.7	6.63 ± 0.47	6.47 ± 0.30	6.21 ± 0.25	1.47 ± 0.07	1.52 ± 0.08	
	0.8	6.27 ± 0.41	6.20 ± 0.32	6.23 ± 0.31	1.45 ± 0.07	1.48 ± 0.07	
	0.9	6.46 ± 0.32	6.19 ± 0.35	6.42 ± 0.28	1.41 ± 0.07	1.43 ± 0.07	
Average		6.5 ± 0.4	6.3 ± 0.3	6.3 ± 0.3	1.44 ± 0.07	1.48 ± 0.07	1.43
A482-S358	0.1	6.40 ± 0.60	6.30 ± 0.40	6.50 ± 0.60	1.28 ± 0.05	1.31 ± 0.05	
	0.2	5.92 ± 0.63	6.03 ± 0.44	6.81 ± 0.67	1.34 ± 0.05	1.32 ± 0.05	
	0.3	6.05 ± 0.61	6.14 ± 0.42	7.50 ± 0.58	1.37 ± 0.05	1.32 ± 0.05	
Average		6.1 ± 0.6	6.2 ± 0.4	6.9 ± 0.6	1.34 ± 0.05	1.32 ± 0.05	1.40

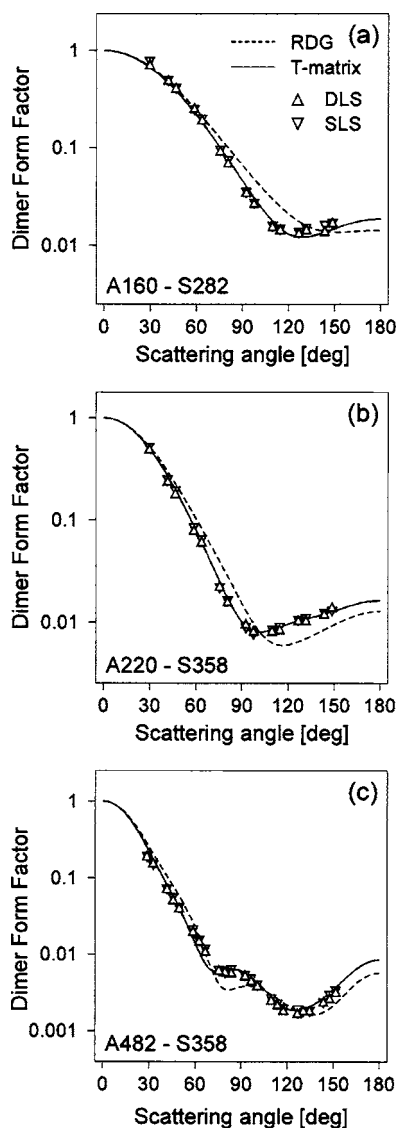


FIG. 5. Comparison of measured form factors for dimers with results of T -matrix calculations (solid line) and RDG theory (dashed line) including effects of polydispersity and back reflection. Different couples are (a) A160-S282 for mole fraction of amidine particles $x_A=0.8$, (b) A220-S358 for $x_A=0.8$, and (c) A482-S358 for $x_A=0.2$. The other mole fractions are not shown, but they follow the data closely.

niques indicates that the T -matrix must provide a good description of the optical properties. A more direct argument of its validity will be given in the following section.

Dimer form factors

Once the heteroaggregation rate constants and hydrodynamic dimer radii are known, we can recalculate the form factors of the dimer from the SLS as well as the DLS data. Knowing the aggregation rate constant and the hydrodynamic factor, the scattered intensity of the dimer $I_{AB}(q)$ can then be extracted from either Eq. (3) or Eq. (5). Since the absolute value of the forward dimer-scattered intensity $I_{AB}(q=0)$ is not experimentally accessible, this quantity is reported as the dimer form factor, which is normalized to unity for small scattering angles. The latter is compared with the dimer form factors calculated with the superposition T -matrix method.

The measured dimer form factors are shown in Fig. 5 for the respective pairs A160-S282, A220-S358, and A482-S358. The good agreement between the SLS and DLS data is a strong indication of the consistency of the presented data analysis. The experimental results are compared with the calculations based on the superposition T -matrix method (solid line) and the RDG approximation (dashed line). Both calculations invoke corrections due to polydispersity and back reflection. Consideration of the back reflection is essential, especially for the larger particles, which scatter strongly in the forward direction.

For the smallest couple A160-S282 shown in Fig. 5(a), the differences between the superposition T -matrix calculation and RDG approximation are relatively minor. Nevertheless, the superposition T -matrix calculation captures the angle dependence more accurately. For the medium-sized couple A220-S358 shown in Fig. 5(b), the discrepancies between the superposition T -matrix calculation and RDG approximation are considerable, but the experimental data is very well captured by the T -matrix method. The effects of polydispersity are small in this case, since the particles are relatively monodisperse. For the largest couple A482-S358 shown in Fig. 5(c), the superposition T -matrix calculation and RDG approximation for monodisperse samples yield qualitatively different predictions, as evidenced by the different number of minima accessible in the angular range. Nevertheless, the superposition T -matrix theory captures the data extremely well over almost three orders of magnitude in scattering intensity.

These results demonstrate that the superposition T -matrix method predicts the form factors of asymmetric dimer of latex particles in the submicrometer range extremely well. For latex particle dimer in aqueous suspensions, the RDG approximation is only accurate up to particle diameters of about 250 nm. This finding is in accordance with earlier findings of symmetric dimers.⁶

CONCLUSION

In a dilute aqueous suspension of mixed positively and negatively charged latex particles at low salt concentration, aggregate dimers of oppositely charged particles form. When one follows such an aggregation process with time-resolved light scattering, the form factors of asymmetric particle dimers can be extracted from its short-time behavior. These experimental form factors are compared with independent calculations based on the superposition T -matrix method and RDG approximation. While the RDG approximation is found to be valid up to particle diameters of about 250 nm, the superposition T -matrix method is very accurate for all types of dimers investigated.

To our knowledge, the present measurements of form factors of asymmetric particle dimers are the first of its kind. The results clearly show the appropriateness of the superposition T -matrix method to accurately estimate the optical properties of colloidal particles in the micrometer range.

ACKNOWLEDGMENTS

This work was supported by the Swiss National Science Foundation and the University of Geneva. One of the authors (M.M.) acknowledges support from the NASA Radiation Sciences Program managed by Hal Maring.

¹E. Matijevic, *Chem. Mater.* **5**, 412 (1993).

²L. M. Liz-Marzan, M. Giersig, and P. Mulvaney, *Langmuir* **12**, 4329 (1996).

³D. G. Shchukin, G. B. Sukhorukov, and H. Mohwald, *Angew. Chem., Int. Ed.* **42**, 4472 (2003).

⁴A. I. Petrov, A. A. Antipov, and G. B. Sukhorukov, *Macromolecules* **36**, 10079 (2003).

⁵M. Elimelech, J. Gregory, X. Jia, and R. A. Williams, *Particle Deposition and Aggregation: Measurement, Modeling, and Simulation* (Butterworth-Heinemann, Oxford, 1995).

⁶H. Holthoff, M. Borkovec, and P. Schurtenberger, *Phys. Rev. E* **56**, 6945 (1997).

⁷H. Holthoff, S. U. Egelhaaf, M. Borkovec, P. Schurtenberger, and H. Sticher, *Langmuir* **12**, 5541 (1996).

⁸H. Wu, S. Lodi, and M. Morbidelli, *J. Colloid Interface Sci.* **256**, 304 (2002).

⁹D. A. Weitz, J. S. Huang, M. Y. Lin, and J. Sung, *Phys. Rev. Lett.* **54**, 1416 (1985).

¹⁰J. Hansen, M. Sato, R. Ruedy, A. Lacis, and V. Oinas, *Proc. Natl. Acad. Sci. U.S.A.* **97**, 9875 (2000).

¹¹M. I. Mishchenko, B. Cairns, J. E. Hansen, L. D. Travis, R. Burg, Y. J. Kaufman, J. V. Martins, and E. P. Shettle, *J. Quant. Spectrosc. Radiat. Transf.* **88**, 149 (2004).

¹²C. Bohren and D. R. Huffman, *Absorption and Scattering of Light by Small Particles* (Wiley Interscience, New York, 1983).

¹³M. I. Mishchenko, L. D. Travis, and A. A. Lacis, *Scattering, Absorption, and Emission of Light by Small Particles* (Cambridge University Press, Cambridge, 2002).

¹⁴E. M. Purcell and C. R. Pennypacker, *Astrophys. J.* **186**, 705 (1973).

¹⁵B. T. Draine and P. J. Flatau, *J. Opt. Soc. Am. A* **11**, 1491 (1994).

¹⁶D. W. Mackowski and M. I. Mishchenko, *J. Opt. Soc. Am. A* **13**, 2266 (1996).

¹⁷M. I. Mishchenko and D. W. Mackowski, *Opt. Lett.* **19**, 1604 (1994).

¹⁸K. A. Fuller, G. W. Kattawar, and R. T. Wang, *Appl. Opt.* **25**, 2521 (1986).

¹⁹R. T. Wang, J. M. Greenberg, and D. W. Schuerman, *Opt. Lett.* **6** (1981).

²⁰M. I. Mishchenko and D. W. Mackowski, *J. Quant. Spectrosc. Radiat. Transf.* **55**, 683 (1996).

²¹W. L. Yu, E. Matijevic, and M. Borkovec, *Langmuir* **18**, 7853 (2002).

²²P. Galletto, W. Lin, and M. Borkovec, *Phys. Chem. Chem. Phys.* **7**, 1464 (2005).